

FORMING CIRCUMNUCLEAR DISKS AND RINGS IN GALACTIC NUCLEI: A COMPETITION BETWEEN SUPERMASSIVE BLACK HOLE AND NUCLEAR STAR CLUSTER

ALESSANDRO A. TRANI^{1,2,3,*†}, MICHELA MAPELLI^{3,4}, AND ALESSANDRO BALLONE³

Draft version July 27, 2018

Abstract

We investigate the formation of circumnuclear gas structures from the tidal disruption of molecular clouds in galactic nuclei, by means of smoothed particle hydrodynamics simulations. We model galactic nuclei as composed of a supermassive black hole (SMBH) and a nuclear star cluster (NSC) and consider different mass ratios between the two components. We find that the relative masses of the SMBH and the NSC have a deep impact on the morphology of the circumnuclear gas. Extended disks form only inside the sphere of influence of the SMBH. In contrast, compact rings naturally form outside the SMBH's sphere of influence, where the gravity is dominated by the NSC. This result is in agreement with the properties of the Milky Way's circumnuclear ring, which orbits outside the SMBH sphere of influence. Our results indicate that compact circumnuclear rings can naturally form outside the SMBH sphere of influence.

Subject headings: ISM: clouds – black hole physics – ISM: kinematics and dynamics – methods: numerical – galaxies: nuclei – galaxies: star clusters: general

1. INTRODUCTION

Galactic nuclei (GNs) can be remarkably rich in molecular gas. An increasing number of observations reveal the presence of circumnuclear gas in the innermost parsecs of nearby GNs, where the gravity is dominated by a supermassive black hole (SMBH, Neumayer et al. 2007; Tristram et al. 2009; Seth 2010; Davis et al. 2013; Menezes et al. 2013; Menezes & Steiner 2015; Onishi et al. 2015; Barth et al. 2016a,b; Onishi et al. 2017; Davis et al. 2017; Espada et al. 2017).

Molecular gas is also present in Milky Way's Galactic center (GC), where a dusty molecular torus - the so-called circumnuclear ring⁷ (CNR) - orbits at about 2 pc from the SMBH (Serabyn et al. 1986; Wright et al. 2001; Christopher et al. 2005; Oka et al. 2011; Liu et al. 2012, 2013; Mills et al. 2013; Goicoechea et al. 2013; Smith & Wardle 2014; Harada et al. 2015; Takekawa et al. 2017; Mills et al. 2017; Sandqvist et al. 2017; Goicoechea et al. 2018).

¹ Department of Astronomy, Graduate School of Science, The University of Tokyo, 7-3-1 Hongo, Bunkyo-ku, Tokyo, 113-0033, Japan

² Scuola Internazionale Superiore di Studi Avanzati (SISSA), Via Bonomea 265, I-34136, Trieste, Italy

³ INAF-Osservatorio Astronomico di Padova, Vicolo dell'Osservatorio 5, I-35122, Padova, Italy

⁴ Institute for Astrophysics and Particle Physics, University of Innsbruck, Technikerstrasse 25/8, A-6020, Innsbruck, Austria
* Email: aatrani@gmail.com

† JSPS Fellow

⁷ In the literature the CNR can be sometimes referred as "circumnuclear disk" or "torus". In our manuscript, we define a flattened gas structure as a "ring" if it has a significant hole in its center. This definition was adopted to simplify the notation in the manuscript, i.e. to clearly distinguish between a disk (without hole) and a ring. According to e.g. Liu et al. (2013) the CNR extends from ~ 1.5 –2 pc to 3–4 pc and it has a clear "hole" in the centre. In addition, the CNR has an asymmetric, 7pc-long extension towards negative galactic longitude. This extension may be a remnant of the parent molecular cloud that has been captured and disrupted by the potential well at the nucleus. For example, see figure 7 of Takekawa et al. 2017.

Circumnuclear gas exhibits a complex morphology and kinematics, with clumpy streamers, warped rings and/or disks that deviate from axisymmetry and circular motion. How the complex spatial and velocity structure of circumnuclear gas forms and evolves remains poorly understood. This uncertainty limits the use of molecular gas dynamics to infer the dynamical mass of SMBHs, a method that is recently emerging thanks to high-resolution sub-millimeter interferometry (Davis 2014; Yoon 2017).

Furthermore, circumnuclear gas may form stars in the close proximity to SMBHs (Poliachenko & Shukhman 1977; Kolykhalov & Syunyaev 1980; Shlosman & Begelman 1987; Sanders 1998; Collin & Zahn 1999; Gammie 2001; Levin & Beloborodov 2003; Goodman 2003; Milosavljević 2004; Nayakshin & Cuadra 2005; Nayakshin et al. 2007; Cuadra et al. 2008; Collin & Zahn 2008; Yusef-Zadeh et al. 2012, 2013, 2015, 2017a,b). Evidence comes from the observations of young stars orbiting around the SMBH in the GC and in M31 (e.g. Ghez et al. 2003; Schödel et al. 2003; Eisenhauer et al. 2005; Paumard et al. 2006; Gillessen et al. 2009b; Bartko et al. 2009; Do et al. 2013; Yelda et al. 2014; Feldmeier-Krause et al. 2015; Tremaine 1995; Bender et al. 2005; Lauer et al. 2012; Menezes et al. 2013; Brown & Magorrian 2013; Lockhart et al. 2017).

Similar episodes of star formation in the central parsecs are expected to be detected in other nearby galaxies with the advent of 30-meter telescopes (Gullieuszik et al. 2014; Do et al. 2014; Carson et al. 2015). Young, luminous stars such as the ones we observe in the Milky Way's GC are excellent candidates to infer the SMBH mass from kinematic measurements (Schödel et al. 2002; Ghez et al. 2003; Gillessen et al. 2009a). Such stars may even retain the dynamical properties of the parent gas and thus help to constrain the past history of the GN (Mapelli 2017).

Circumnuclear gas may form from the tidal disruption of giant molecular clouds. This scenario has been studied in detail in the context of the GC and can explain

TABLE 1
MAIN PROPERTIES OF THE SIMULATIONS.

Run	$M_{\text{tot}} [M_{\odot}]$	$M_{\text{SMBH}} [M_{\odot}]$	f_{SMBH}	$R_{\text{SOI}} [\text{pc}]$	$m_{\text{res}} [M_{\odot}]$
mt5e7_bh2.5e7	5×10^7	2.5×10^7	0.5	>10	0.5
mt5e7_bh1e7	5×10^7	1×10^7	0.2	0.90	0.5
mt5e7_bh5e6	5×10^7	5×10^6	0.1	0.35	0.5
mt5e7_bh2.5e6	5×10^7	2.5×10^6	0.05	0.15	0.5
mt1e7_bh5e6	1×10^7	5×10^6	0.5	>10	0.5
mt1e7_bh2e6	1×10^7	2×10^6	0.2	0.90	0.5
mt1e7_bh1e6	1×10^7	1×10^6	0.1	0.35	0.5
mt1e7_bh5e5	1×10^7	5×10^5	0.05	0.15	0.5
mt5e6_bh2.5e6	5×10^6	2.5×10^6	0.5	>10	0.5
mt5e6_bh1e6	5×10^6	1×10^6	0.2	0.90	0.5
mt5e6_bh5e5	5×10^6	5×10^5	0.1	0.35	0.5
mt5e6_bh2.5e5	5×10^6	2.5×10^5	0.05	0.15	0.5
mt1e7_bh5e6_hr	1×10^7	5×10^6	0.5	>10	0.05
mt5e6_bh1e6_hr	5×10^6	1×10^6	0.2	0.35	0.05
mt5e7_bh1e6_hr	5×10^7	1×10^6	0.02	0.06	0.05

Column 1: run name; column 2: mass enclosed in a 10 pc radius M_{tot} in M_{\odot} , composed of the NSC and the SMBH; column 3: mass of the SMBH M_{SMBH} in M_{\odot} ; column 4: f_{SMBH} ; column 5: radius of sphere of influence R_{SOI} of the SMBH in pc; m_{res} is the mass resolution of the simulation in M_{\odot} .

(i) the formation of the CNR and (ii) the young stellar disk (Wardle & Yusef-Zadeh 2008; Bonnell & Rice 2008; Hobbs & Nayakshin 2009; Lucas et al. 2013; Trani et al. 2016; Mapelli & Trani 2016). However, little attention has been paid to this scenario in GNs with different properties from those of the Milky Way.

In general, the outcome of a cloud tidal disruption depends on details of the central gravitational field. SMBHs are commonly thought to dominate the gravitational field of the central parsecs. On the other hand, many GNs host a massive and compact stellar cluster at their center - the so-called nuclear star cluster (NSC) -, whose mass is also a fundamental component of the central potential well. NSCs and SMBHs may even co-exist in the same GN.

In fact, many GNs host a compact, massive stellar cluster at their center, and both NSCs and SMBHs may coexist in the same GN (Böker et al. 2002, 2004; Côté et al. 2006; Georgiev & Böker 2014; den Brok et al. 2014; Georgiev et al. 2016; Nguyen et al. 2017).

The most striking example is in the GC, where the NSC contains twice the mass of the SMBH at only ~ 2 pc (Schödel et al. 2007; Graham & Spitler 2009; Schödel et al. 2009; Yusef-Zadeh et al. 2012; Schödel et al. 2014; Feldmeier et al. 2014; Chatzopoulos et al. 2015; Fritz et al. 2016; Gallego-Cano et al. 2017; Schödel et al. 2017; Feldmeier-Krause et al. 2017).

The mass ratio between SMBH and NSC can vary widely from galaxy to galaxy, consequently affecting the shape of the central potential. This is expected to have a strong impact in the disruption of nearby molecular clouds and hence might shape the properties of circumnuclear gas.

In this paper, we present the first systematic study on the formation of gaseous circumnuclear rings/disks in GNs with properties different from those of the GC. We simulate the infall of a molecular cloud towards the central potential of GNs, composed of a SMBH and the cusp of a NSC. We run a grid of smoothed-particle hydrodynamics (SPH) simulations by varying the mass ratio between the SMBH and the stellar cusp, and study the

From the values of the SMBH mass and the NSC cusp

properties of the resulting distribution of gas.

Section 2 describes the numerical methods we employed for our simulations. Section 3 presents the main results from the simulations. In Section 4, we discuss the impact of the SMBH to NSC mass ratios on circumnuclear gas morphology and its implications for SMBH mass measurement. Finally, our conclusions are summarized in Section 5.

2. METHODS

We use the N-body/SPH code Gasoline2 (Wadsley et al. 2004; Read et al. 2010; Wadsley et al. 2017) to simulate the infall and disruption of a molecular cloud in the central parsecs of GNs.

We consider GNs as composed of a stellar cusp and a central SMBH. The SMBH is a sink particle of mass M_{SMBH} whose position is fixed at the center; in this way we avoid spurious random walk due to numerical effects.

The stellar cusp of the NSC is modeled as a spherical potential and follows a broken power-law density profile:

$$\rho(r) = \rho_0 \left(\frac{r}{r_0} \right)^{-\gamma} \quad (1)$$

We use the values given by Schödel et al. (2007) for the cusp of the Milky Way: $\gamma = 1.75$ for $r > r_0$ and $\gamma = 1.2$ for $r < r_0$, where $r_0 = 0.22$ pc. The cusp is truncated at $r_{\text{trunc}} = 100$ pc and has a total mass M_{cusp} . We choose ρ_0 in the following way: first we choose the SMBH mass (M_{SMBH}) and the total mass of the GN within 10 pc [$M_{\text{tot}} = M_{\text{cusp}}(<10 \text{ pc}) + M_{\text{SMBH}}$]. Then we pick ρ_0 so that $M_{\text{cusp}}(<10 \text{ pc}) = \int_0^{10 \text{ pc}} 4\pi\rho(r)r^2 dr = M_{\text{tot}} - M_{\text{SMBH}}$.

We have run three sets of simulations, each with a different value of M_{tot} : 5×10^7 , 1×10^7 and $5 \times 10^6 M_{\odot}$. For each set we have run four simulations choosing M_{SMBH} so that $f_{\text{SMBH}} = M_{\text{SMBH}}/M_{\text{tot}} = 0.5, 0.2, 0.1$ and 0.05 . This choice allows us explore the parameter space of SMBH and NSC masses in a range consistent with the observations (Seth et al. 2008; Graham & Spitler 2009; Kornei & McCrady 2009; Kormendy & Ho 2013; Georgiev & Böker 2014; Georgiev et al. 2016).

profile, we derive the radius of the sphere of influence

of the SMBH R_{SOI} . Although usually the sphere of influence is defined as the region enclosing a total mass twice that of the SMBH mass, this definition is valid only for an isothermal sphere model of the NSC. Therefore, R_{SOI} is computed numerically from the equation $\Phi_{\text{SMBH}} = \Phi_{\text{cusp}}$, where Φ_{SMBH} and Φ_{cusp} are the gravitational potential of the SMBH and of the cusp, respectively. Table 1 summarizes the main properties of the simulations presented in this paper.

In all simulations, the molecular cloud is modeled as a homogeneous gas sphere of $10^5 M_{\odot}$ and 15 pc radius, located at 26 pc from the SMBH. The cloud is seeded with turbulent velocity and marginally self-bound. The velocity field is generated using a grid method (Dubinski et al. 1995) from a divergence-free, random Gaussian field with a power spectrum $P(k) = \|\delta v_k\|^2 \propto k^{-4}$. The spectral index -4 reproduces turbulence in agreement with the velocity dispersion relation $\sigma_v \propto l^{0.5}$ observed in molecular clouds (Larson 1981).

The cloud has an impact parameter of $b = 15$ pc with respect to the SMBH and an initial velocity of $v_i = 0.2v_{\text{esc}}$, where v_{esc} is the escape velocity of the cloud, taking into account the potential of the SMBH and the NSC. The initial velocity is $v_i = 46.7$, 20.1 and 13.7 km s^{-1} in the runs with $M_{\text{tot}} = 5 \times 10^7$, 1×10^7 and $5 \times 10^6 M_{\odot}$, respectively. The coordinate system is chosen so that the total velocity vector lies in the x - y

plane. The mass of the gas particles is $m_{\text{res}} = 0.05 M_{\odot}$ in high-resolution runs and $0.5 M_{\odot}$ in every other runs. We stop the simulations at 3 Myr.

Star formation is modeled via sink particle creation, implemented following the criteria of Bate et al. (1995) and Federrath et al. (2010). Specifically, a gas particle is considered a sink candidate if it exceeds a threshold density ρ_{thr} . We choose $\rho_{\text{thr}} = 10^{-16} \text{ g cm}^{-3}$. We performed tests to ensure that different values of ρ_{thr} do not impact significantly on the mass function of the formed sink particles. We set a sink accretion radius of $r_{\text{accr}} = 1.5 \times 10^{-3}$ pc. The gravitational softening length is chosen to be 7.93×10^{-4} pc and 3.68×10^{-4} pc in runs with $m_{\text{res}} = 0.5 M_{\odot}$ and $m_{\text{res}} = 0.05 M_{\odot}$, respectively.

We employ the Cullen & Dehnen (2010) viscosity limiter, which uses the total time derivative of the velocity divergence as shock indicator.

All simulations include the radiative cooling algorithm described in Boley (2009) and Boley et al. (2010). The cooling is calculated from $\nabla \dot{F} = -(36\pi)^{1/3} s^{-1} \sigma (T^4 - T_{\text{irr}}^4) (\Delta\tau + 1/\Delta\tau) - 1$, where $s = (m/\rho)^{1/3}$ and $\Delta\tau = sk\rho$, for the local opacity k , particle mass m , and density ρ . D'Alessio et al. (2001) opacities are used, with a $1 \mu\text{m}$ maximum grain size. The irradiation temperature is $T_{\text{irr}} = 100$ K everywhere.

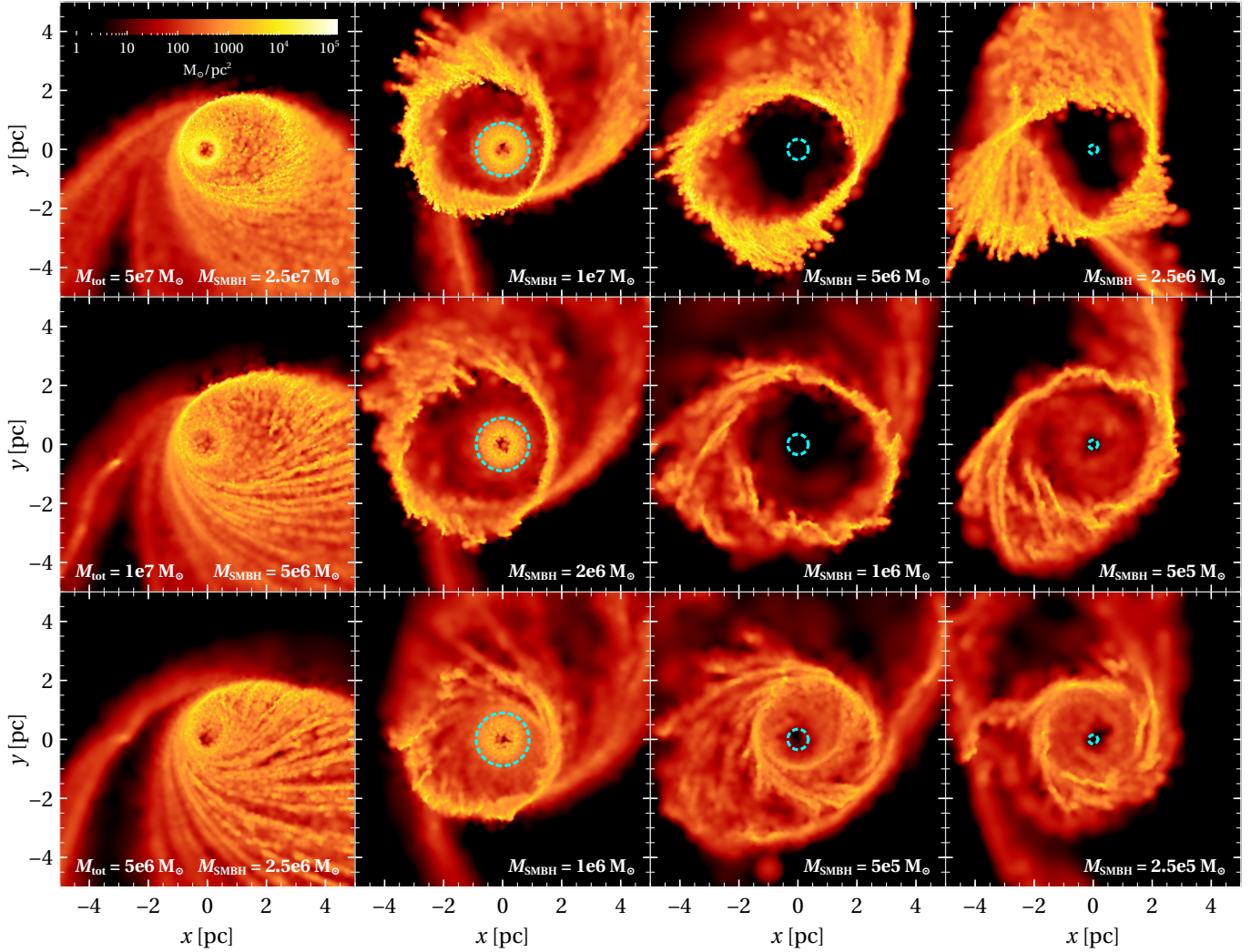


FIG. 1.— Color-coded, projected density map of gas in the x - y plane for the three sets of runs (rows), comprising of four initial setups (columns, see Table 1). Each panel corresponds to a different simulation. From top to bottom, each row has $M_{\text{tot}} = M_{\text{cusp}} + M_{\text{SMBH}}$ of 5×10^7 , 1×10^7 and $5 \times 10^6 M_{\odot}$, respectively. From left to right, each column has $f_{\text{SMBH}} = M_{\text{SMBH}}/M_{\text{tot}} = 0.5, 0.2, 0.1$ and 0.05 . The dashed cyan circle indicates the SMBH radius of influence R_{SOBH} . From top to bottom, each row corresponds to a time of 0.6, 1.5 and 2 Myr from the start of the simulations. Bottom row snapshots are taken at a later times because the gas cloud evolves more slowly in simulations with lower M_{tot} . R_{SOBH} is not shown in the left-hand panels because it is larger than the box.

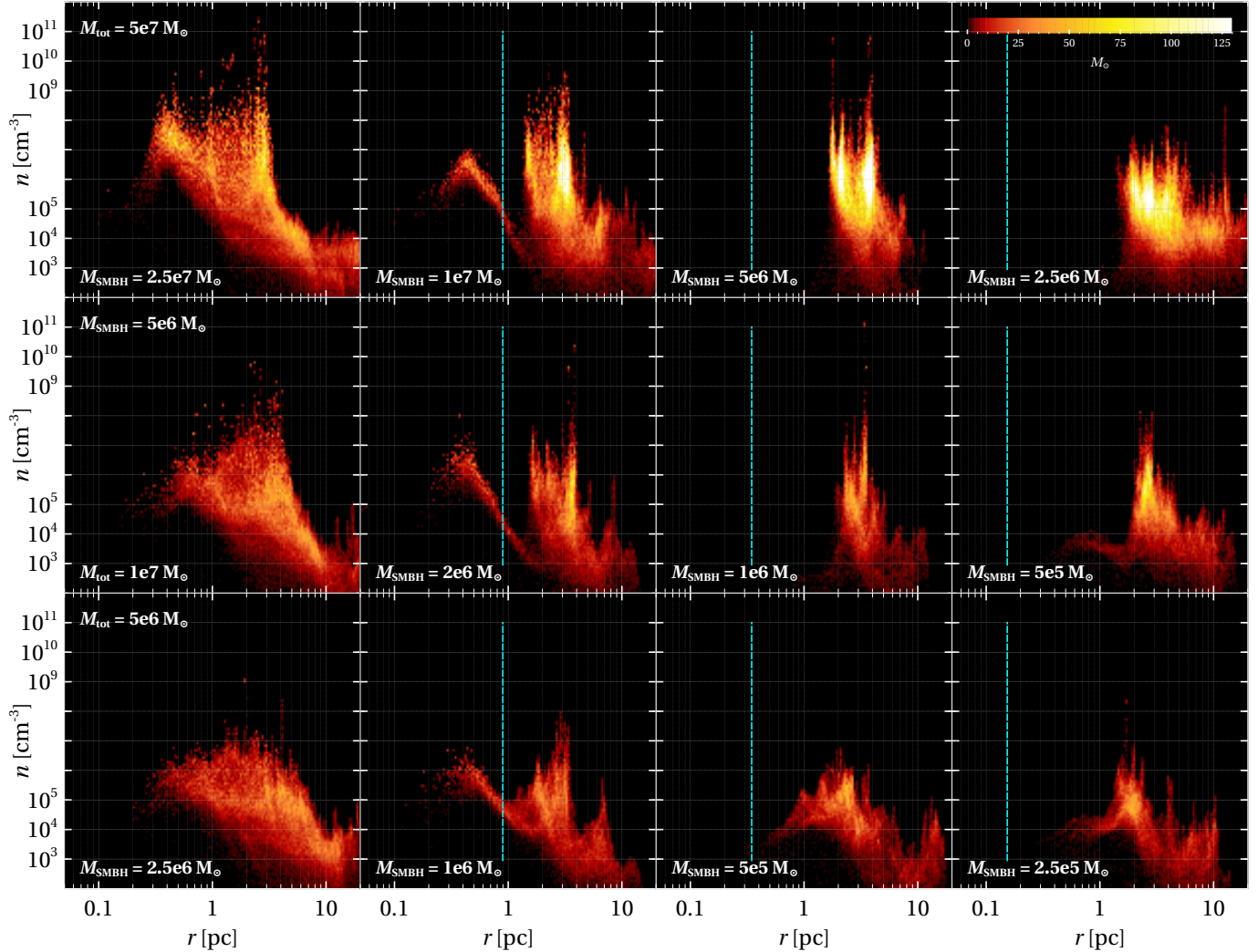


FIG. 2.— Number density of gas as a function of distance from the central SMBH for all snapshots of Figure 1. The color scale indicates the gas mass in the radial-density bin. The cyan dashed line is the SMBH influence radius R_{SOI} . Each panel corresponds to a different simulation. From top to bottom, each row has $M_{\text{tot}} = M_{\text{cusp}} + M_{\text{SMBH}}$ of 5×10^7 , 1×10^7 and $5 \times 10^6 M_\odot$, respectively. From left to right, each column has $f_{\text{SMBH}} = M_{\text{SMBH}}/M_{\text{tot}} = 0.5, 0.2, 0.1$ and 0.05 . From top to bottom, each row corresponds to a time of 0.6, 1.5 and 2 Myr from the start of the simulations. Bottom row snapshots are taken at a later times because the gas cloud evolves more slowly in simulations with lower M_{tot} . R_{SOI} is not shown in the left-hand panels because it is larger than the box.

3. RESULTS

From our simulations we study the tidal disruption of the cloud in the tidal field of the SMBH and the NSC. The contribution of the SMBH will dominate the potential inside its influence radius. Thus, we expect that gas reaching the influence radius of the SMBH will settle on a nearly Keplerian orbit around the SMBH. In contrast, the NSC will give the dominant contribution to the potential outside the SMBH influence radius. We expect that gas settling outside the SMBH influence radius will feel mostly the effect of the NSC.

Figure 1 shows the projected density map of the whole grid of simulations at different snapshots. The total mass M_{tot} of the GN decreases from top to bottom, while the ratio between the SMBH mass and the total mass of the GN (f_{SMBH}) decreases from left to right. The morphol-

ogy of the circumnuclear gas shows a clear trend with f_{SMBH} . At $f_{\text{SMBH}} = 0.5$, the whole cloud gets flattened into an eccentric, extended disk around the SMBH. As the mass of the SMBH becomes lower with respect to that of the NSC ($f_{\text{SMBH}} \leq 0.2$), the gas gets squeezed into a compact ring outside the sphere of influence of the SMBH. A disk of material captured by the SMBH potential resides within the cavity of the ring in the runs with $f_{\text{SMBH}} = 0.2$. This is clear also from Figure 2, which shows the corresponding radial distribution of the gas density in for all snapshots of Figure 1.

For $f_{\text{SMBH}} < 0.2$, the sphere of influence of the SMBH is too small to allow for the capture of gas particles in our initial condition. A smaller initial velocity and/or impact parameter would lead to the formation of a disk inside R_{SOI} also in these cases (Mapelli & Trani 2016).

TABLE 2
MAIN OUTCOMES OF THE SIMULATIONS.

Run	$r_{\text{disk}}^{\text{in}}$ [pc]	$r_{\text{disk}}^{\text{out}}$ [pc]	M_{disk} [M_{\odot}]	$r_{\text{ring}}^{\text{in}}$ [pc]	$r_{\text{ring}}^{\text{out}}$ [pc]	M_{ring} [M_{\odot}]	M_{stars} [M_{\odot}]	M_{accr} [M_{\odot}]
mt5e7_bh2.5e7	0.23	7.5	7.1×10^4	—	—	—	1.0×10^4	7.0×10^3
mt5e7_bh1e7	0.2	1.0	4.3×10^3	1.4	3.6	4.6×10^4	2.9×10^4	3.9×10^3
mt5e7_bh5e6	—	—	—	1.6	4.0	6.2×10^4	2.4×10^4	2.2×10^3
mt5e7_bh2.5e6	—	—	—	1.7	5.6	5.9×10^4	2.2×10^4	1.7×10^3
mt1e7_bh5e6	0.23	9.2	8.5×10^4	—	—	—	4.6×10^4	6.4×10^3
mt1e7_bh2e6	0.15	0.9	2.8×10^3	1.6	4.0	1.7×10^4	7.1×10^4	3.6×10^3
mt1e7_bh1e6	—	—	—	2.2	3.7	1.2×10^4	8.2×10^4	2.4×10^3
mt1e7_bh5e5	—	—	—	2.1	3.1	1.2×10^4	7.4×10^4	2.3×10^3
mt5e6_bh2.5e6	0.25	9.8	7.9×10^4	—	—	—	5.3×10^4	6.1×10^3
mt5e6_bh1e6	0.17	0.9	5.7×10^3	1.7	3.5	1.1×10^4	7.6×10^4	3.6×10^3
mt5e6_bh5e5	—	—	—	1.3	2.7	8.1×10^3	8.3×10^4	2.8×10^3
mt5e6_bh2.5e5	—	—	—	1.3	2.9	7.7×10^3	8.3×10^4	2.3×10^3

Column 1: run name; column 2: inner radius of the disk in pc; column 3: outer radius of the disk in pc; column 4: disk mass in M_{\odot} ; column 5: inner radius of the ring in pc; column 6: outer radius of the ring in pc; column 7: ring mass in M_{\odot} ; column 8: mass of formed stars in M_{\odot} ; column 9: mass accreted by the SMBH. All quantities refer to the snapshots presented in Figures 1 and 2.

Table 2 summarizes the properties of the disk and the inner ring formed in the simulations after the complete disruption of the cloud, which corresponds to 0.6, 1.5

Figure 3 shows the time evolution of the gas cloud in run `mt5e7_bh1e6_hr` ($f_{\text{SMBH}} = 0.02$, first and second column) and run `mt5e6_bh1e6_hr` ($f_{\text{SMBH}} = 0.2$, third and fourth column). Although the SMBH mass is the same in both runs, the gas follows a very different evolution.

In run `mt5e7_bh1e6_hr` the gas cloud is disrupted more rapidly due to the higher total mass ($M_{\text{tot}} = 5 \times 10^7 M_{\odot}$). During the first 0.5 Myr the gas is stretched into a nearly-radial streamer, in which high-density clumps are formed. Afterwards, the gas begins to fall back, inter-

Conversely, in run `mt5e6_bh1e6_hr`, the trajectory of the infalling gas is deflected by the SMBH gravity and the gas winds up around the SMBH, forming a flattened disk (0.6 Myr). The eccentricity of the disk increases with the distance from the SMBH. The shear arisen at pericenter leads to a rapid circularization of the inner part of the disk, which decouples from the outer part.

At 1.3 Myr, there are two distinct structures: a small disk of ~ 0.2 pc radius around the SMBH and an outer eccentric ring. The external ring is composed of several streamers. The ring precesses because of the cusp potential, so that its pericenter advances along the orbit (in Figure 3 it moves clockwise). The cloud is completely disrupted at ~ 1.7 Myr. The final outcome is a self-interacting, eccentric ring outside R_{SOI} and a dense disk inside R_{SOI} .

The disk that forms around the SMBH has increasing eccentricity for increasing semimajor axis, as shown in the left-hand panel of Figure 4. This feature is an effect of shear viscosity that transports angular momentum outwards, causing the inner parts of the disk to circularize faster. Neighboring streamlines in the disk intersect because of the eccentricity gradient. This gives rise to shocks in the disk (Figure 4, right-hand panel). The shocks tend to damp the eccentricity of the disk, although full circularization ($e = 0$) is never attained in any of the simulations.

About 2–7% of the gas is accreted by the SMBH in all simulations. The accreted mass for each simulation is summarized in Table 2. The lower f_{SMBH} , the less the accreted mass: about $6\text{--}7 \times 10^3 M_{\odot}$ are accreted in the simulations with $f_{\text{SMBH}} = 0.5$, while $1\text{--}2 \times 10^3 M_{\odot}$ are ac-

and 2 Myr from the start of the simulations with $M_{\text{tot}} = 5 \times 10^7$, 1×10^7 and $5 \times 10^6 M_{\odot}$, respectively.

secting the part of the cloud that is still falling towards the center.

At 1 Myr the head of the stream is undergoing a third pericenter passage which is slightly off-set from the first. The streamer follows a rosette-like orbit, which causes it to self-interact and lose eccentricity. At ~ 1.7 Myr the gas cloud has been completely disrupted and has given birth to a clumpy, eccentric ring. The ring shows a large cavity since little gas is captured by the SMBH.

creted in the simulations with $f_{\text{SMBH}} = 0.05$. This value is to be considered as an upper limit since the accretion physics is not resolved at the scale of our simulations.

4. DISCUSSION

The simulations show that the evolution of gas changes drastically depending on the relative masses of SMBH and NSC. The mass ratio between SMBH and NSC determines the radius of the SMBH sphere of influence, R_{SOI} (see fifth column of Table 1), the region in which the dynamics becomes Keplerian. The simulations indicate that gas inside R_{SOI} exhibits a disk morphology, whereas gas settling further out likely forms an eccentric, clumpy ring with characteristics similar to the CNR in the GC.

This is due to the way the tidal potential compresses and shapes the cloud as it gets disrupted. Gas captured in the SMBH sphere of influence tends to wind up around the SMBH, following eccentric Keplerian orbits. This is apparent in the left-hand panel of Figure 5, which shows the trajectory of neighbouring test particles in the gravitational potential of the SMBH and the NSC. If the SMBH potential is dominant, the test particles move on neighbouring Keplerian orbits, forming a precessing disk.

In this case, the gas undergoes circularization through shocks and shear between intersecting disk streamlines. A peculiar feature of this formation mechanism is that the eccentricity of the disk increases from inside out (left-hand panel of Figure 4) and the apsis lines are mutually aligned.

On the other hand, gas that falls into the potential well of the NSC without reaching R_{SOI} is stretched into a nearly radial streamer. This occurs because the gravi-

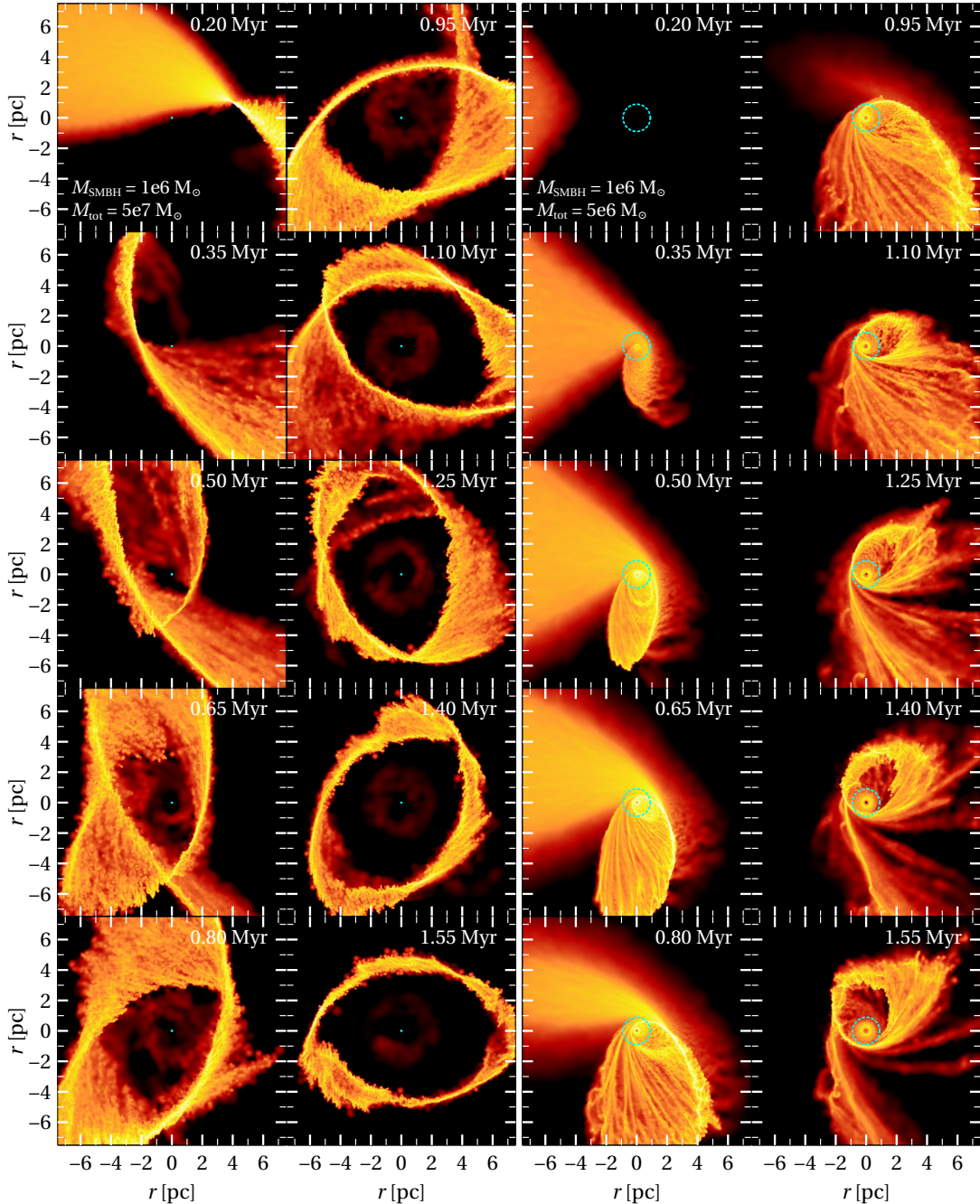


FIG. 3.— Color-coded density map of gas in run `mt5e7_bh1e6_hr` (first and second column) and run `mt5e6_bh1e6_hr` (third and fourth column), projected to the x - y plane of the simulation. From top to bottom and left to right: $t = 0.4, 0.55, 0.7, 0.85, 1, 1.15, 1.3, 1.45, 1.6$ and 1.75 Myr. The dashed cyan circle indicates the SMBH radius of influence R_{SOI} , which is 0.06 and 0.35 pc in run `mt5e7_bh1e6_hr` and `mt5e6_bh1e6_hr`, respectively.

tational acceleration exerted by the NSC scales as $r^{1-\gamma}$, where γ is the density power-law index. Since γ ranges from 1.2 to 1.75 , the acceleration induced by the NSC increases very slowly with r and is not able to strongly alter the orbit of the streamers. This is clear from the right-hand panel of Figure 5, which shows the trajectory of a test particle in a NSC-dominated GN. Test particles follow a wide, self-intersecting rosette orbit. Circularization is induced by the shocks occurring at these self-interactions.

This mechanism can naturally explain why the CNR in the GC presents an inner cavity and does not extend be-

low 1.5 - 2 pc radius (Oka et al. 2011; Liu et al. 2012, 2013; Mills et al. 2013; Smith & Wardle 2014; Harada et al. 2015; Takekawa et al. 2017; Mills et al. 2017; Sandqvist et al. 2017).

Using the mass profile of Genzel et al. (2003a) for Milky Way’s NSC and the mass estimate of (Gillessen et al. 2017) for Sgr A*, the SMBH influence radius turns out to be $R_{\text{SOI}}^{\text{GC}} \simeq 0.4$ pc, much smaller than the inner edge of the CNR.

Another implication is that the formation of compact, CNR-like rings is not expected in GNs lacking a NSC, since the stellar potential would be too shallow to tidally

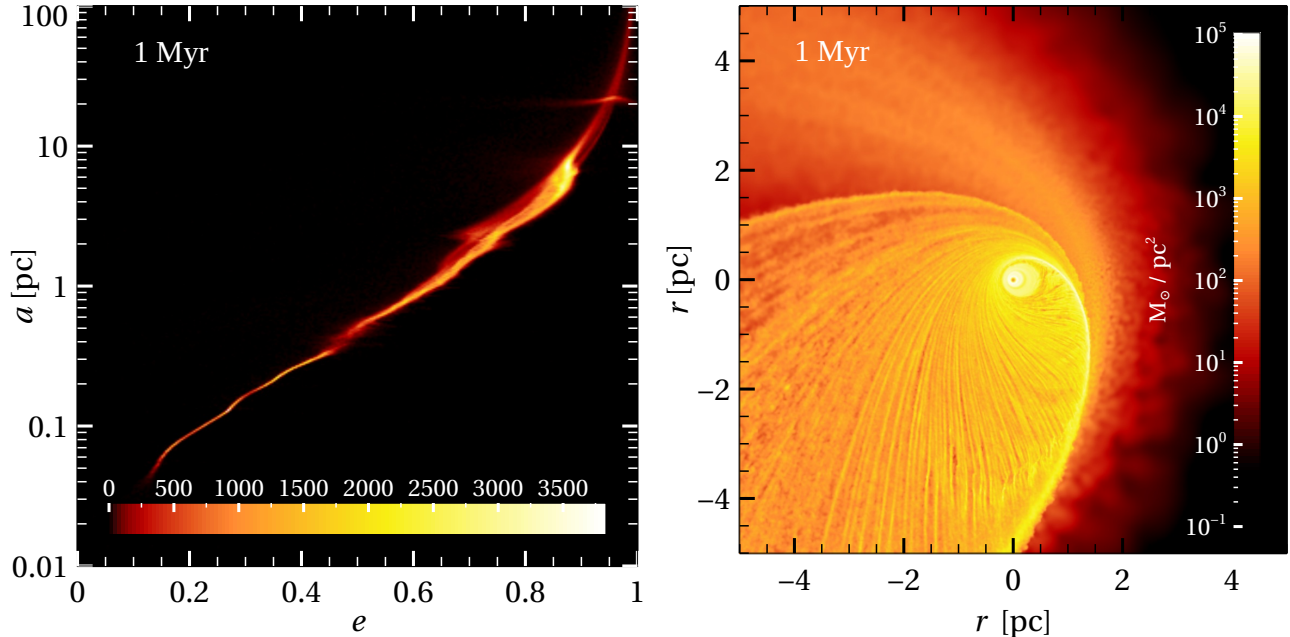


FIG. 4.— Left-hand panel: semimajor axis versus eccentricity for gas particles for run `mt1e7_bh5e6_hr` ($f_{\text{SMBH}} = 0.5$) at 1 Myr. The color scale indicates the number of gas particles. Right-hand panel: color-coded, projected density map of gas in the x - y plane for the same run at the same snapshot.

disrupt a molecular cloud. These findings suggest that the radius of a CNR-like ring in a nucleated GN could be used as an upper limit of the SMBH influence radius (and thus of the SMBH mass), in the hypothesis that the gaseous ring formed according to this mechanism.

Furthermore, $R_{\text{SOI}}^{\text{GC}} \simeq 0.4$ pc is also the outer edge of the so-called clockwise (CW) disk, the disk of young stars around Sgr*A, according to Bartko et al. (2009, (but see also Yelda et al. 2014, who estimate the outer edge at 0.13 pc)). The CW disk might have originated from the fragmentation of an eccentric disk of gas (Nayakshin

Interestingly, the CO brightness distribution in the nucleus of two nearby galaxies, NGC3665 and NGC4429, shows a central gap, which roughly coincides with the estimated R_{SOI} of the central SMBH (see figures 6 of Onishi et al. 2017 and Davis et al. 2018). Based on the results presented here and in Mapelli & Trani (2016), a possible explanation for the deficit of gas inside R_{SOI} is the lack of molecular clouds with angular momentum low enough to be captured by the SMBH gravity and form a disk.

However, the lack of CO emission in the R_{SOI} region of NGC3665 and NGC4429 can be due also to changes of composition in the molecular gas. The simulations presented here do not take into account the evolution of the gas chemistry. In a follow-up study, we will include non-equilibrium chemistry, which will allow us to follow the formation and destruction of H_2 and CO self-consistently throughout the simulations. A systematic comparison between our models and observations of other nearby GNs will be discussed in a forthcoming paper.

4.1. Caveats

In this study, we did not examine the impact of the initial orbit and intrinsic properties of the molecular cloud on the formation of circumnuclear gas, which was instead investigated in Mapelli & Trani (2016). Mapelli & Trani

et al. 2007; Bonnell & Rice 2008; Mapelli et al. 2008; Hobbs & Nayakshin 2009; Alig et al. 2011; Mapelli et al. 2012; Lucas et al. 2013). This picture is consistent with the scenario presented here, in which an eccentric gaseous disk is expected to form at $r \lesssim R_{\text{SOI}}$ if a gas cloud penetrates the SMBH sphere of influence.

These results also indicate that it is difficult to form a gaseous disk close to the SMBH without forming a ring outside R_{SOI} , unless the cloud is compact enough to fit entirely inside R_{SOI} . This strengthens the idea that both the CNR and the CW disk formed from a single molecular cloud disruption episode (Mapelli & Trani 2016). (2016) found that the initial angular momentum of the cloud determines the radius of the outer rings. A higher initial velocity v_i will lead to a larger outer ring, and viceversa. Therefore, we expect that the initial velocity will determine whether gas can reach R_{SOI} and form a disk or not.

Similarly, we expect some dependence on the initial molecular cloud size since the cloud size determines the spread in initial angular momentum of individual gas particles. A larger gas cloud will allow for the formation of an inner disk even for higher total angular momentum, while a more compact cloud will not deposit gas close to the SMBH unless the initial angular momentum is already very low. More discussion about the initial conditions can be found in Appendix A.

Given enough time, the gas viscosity may affect the radial density profile of the disk inside R_{SOI} . We computed the viscous timescale t_{visc} from the properties of the gas in the simulations. The viscous timescale of the inner disk ranges from 4.5 Myr to 165 Myr for a viscosity parameter $\alpha = 0.1$, while for the rings is longer than 200 Myr. This is much longer than the duration of our simulations.

In our simulations, the density profile of the NSC is modelled as in Milky Way's NSC, i.e. as broken-power

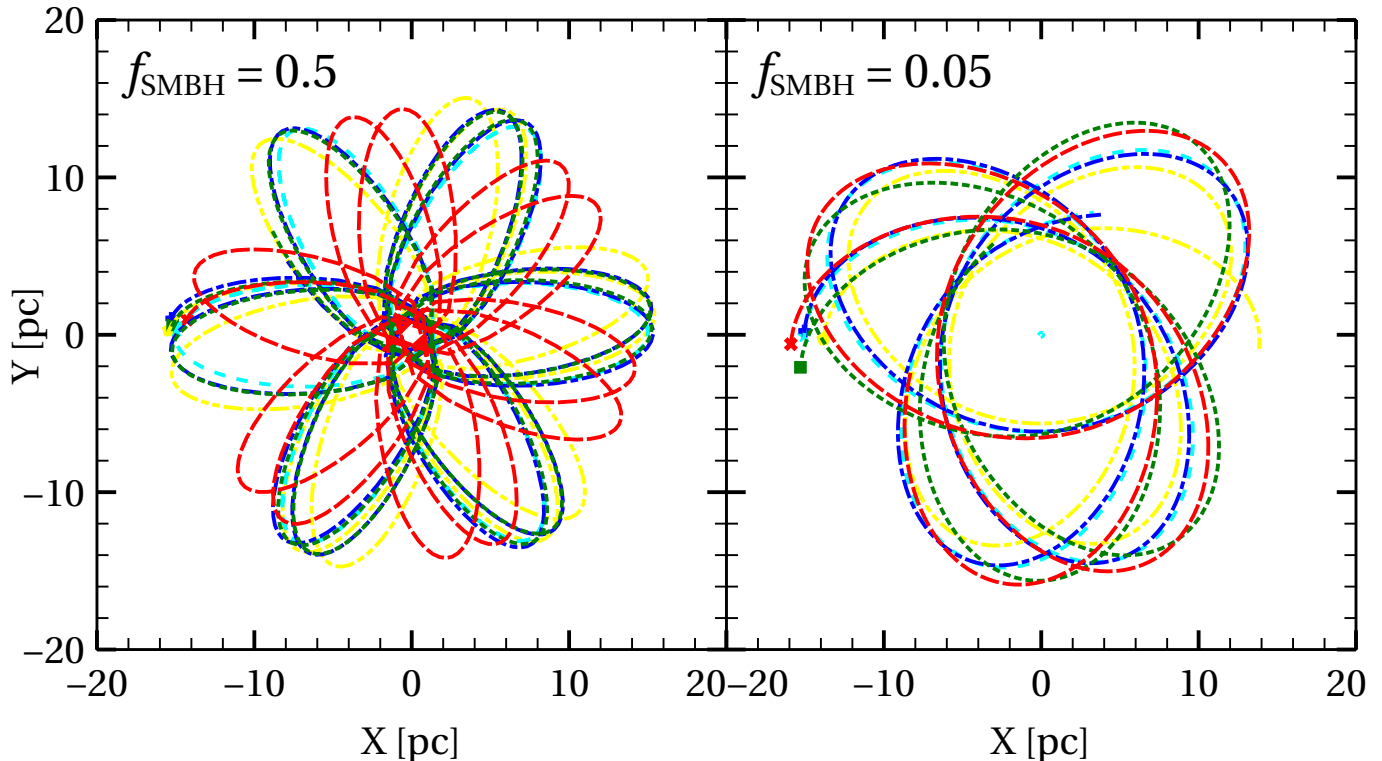


FIG. 5.— Trajectories of 5 test particles in the gravitational potential of the SMBH and NSC. Left-hand panel: $M_{\text{SMBH}} = 2.5 \times 10^7 M_{\odot}$, $M_{\text{tot}} = 5 \times 10^7 M_{\odot}$ ($f_{\text{SMBH}} = 0.5$). Right-hand panel: $M_{\text{SMBH}} = 2.5 \times 10^6 M_{\odot}$, $M_{\text{tot}} = 5 \times 10^7 M_{\odot}$ ($f_{\text{SMBH}} = 0.05$). Each particle has a different color and line type. The initial position is close to $X, Y = (-15, 0)$ pc and it is indicated by a marker. In both panels the particles are evolved for 3 Myr.

law cusped profile (Genzel et al. 2003b). While this is a conservative choice, the density profile of extra-galactic NSCs might be different. Present-day observations are not able to resolve in detail the luminosity profile at the very centre of NSCs, and in recent surveys the surface brightness profiles of NSCs were fitted with a cored King (1962) model (Georgiev & Böker 2014; Georgiev et al. 2016).

Even so, a SMBH embedded into a star cluster is expected to develop a stellar cusp in about a relaxation time, which can be below one Hubble time for NSCs (Bahcall & Wolf 1976). Bahcall & Wolf (1977) predicted the cusp power-law index to be between 1.5 and 2 for a realistic multi-mass cluster. This is consistent with the values adopted in this work.

Moreover, since the mechanism described in this work arises from the shape of the potential rather than its overall depth (i.e. total mass of SMBH plus NSC), it is expected to hold also for mass regimes not probed by the simulations ($M_{\text{tot}} \gtrsim 10^7 M_{\odot}$).

A missing ingredient in this study is the feedback from stars formed in the course of the simulation. The main results presented here are based solely on the dynamics of gas, which could be in principle affected by supernovae, photoionization and outflows from protostars (Pelupessy & Portegies Zwart 2012; Dale et al. 2015).

While the cusp of the NSC is mainly composed of old stellar population, young stars can form from the infalling gas cloud. Indeed, in our simulations the gas fragments and forms stars (or pre-stellar cores), modelled as

sink particles. We will study the dynamics and evolution of stars formed in the simulations in a forthcoming paper.

Nonetheless, the bulk of star formation occurs at 1 Myr, when the gas has already settled long before the first supernovae may explode. In addition, most stars quickly decouple from their parent gas stream and form a distinct, spatially separated structure. Therefore, their impact on the gas through stellar feedback would be limited. More details on the dynamics of stars formed in the simulations will be presented in our next work.

More importantly, the cloud is quickly compressed by tidal forces into streams of dense gas. To alter the gas dynamics, the stellar feedback has to induce a velocity comparable to the gas orbital velocity in the GN potential, which exceeds $\sim 100 \text{ km s}^{-1}$. We thus expect the impact of stellar feedback on the molecular gas to be limited.

A massive O-type star embedded in the gas of our simulations would have Strömgren sphere of radius $\lesssim 5 \times 10^{-3}$ pc. Although the Strömgren radius is rather small compared to the typical size of the gas structures, a fraction of the molecular gas might still get ionized by the stellar radiation. Ionized gas is much more sensible to radiative forces and as such it might display significant deviations from the molecular gas dynamics. One example is the so-called minispiral, a complex of ionized gas filaments that resides in the cavity of the CNR in the GC.

These aspects will be tackled in a forthcoming work,

which will include a better treatment of the gas chemistry. In the present paper, we focus only on the dynamics of molecular gas, which is also a better tracer of the underlying gravitational potential.

5. SUMMARY

We have investigated the formation of circumnuclear disks/rings in GNs with properties different from those of the GC, by means of SPH simulations. We simulated the infall and disruption of a molecular gas cloud towards the central parsecs of a GN, composed of a NSC and a SMBH.

We find that the mass ratio between the SMBH and the NSC has a deep impact on the dynamics of circumnuclear gas. Specifically, circumnuclear gas exhibits different morphology depending on whether it settles inside or outside the radius of influence R_{SOI} of the SMBH.

An extended gaseous disk forms only within R_{SOI} , where the gravity of the SMBH dominates over that of the NSC. Gas that falls within R_{SOI} winds up around the SMBH forming a flattened, eccentric disk. The disk is asymmetric and has an eccentricity that increases with increasing semimajor axis. The disk undergoes circularization due to the eccentricity gradient, which makes neighboring streamlines intersect and shock.

In contrast, compact gaseous rings form only outside the influence radius of the SMBH. Gas that falls outside R_{SOI} is stretched into a nearly-radial streamer by the tidal potential of the NSC. The streamer follows a

rosette-like orbit and undergoes circularization through self-interaction. Eventually, a clumpy, eccentric ring (or annulus) at radii larger than R_{SOI} .

The different evolution of the gas inside and outside R_{SOI} can explain why the inner edge of the CNR in the GC is at large distance from Sgr A* sphere of influence $R_{\text{SOI}}^{\text{GC}} \simeq 0.4 \text{ pc}$.

These findings indicate that the formation of compact rings of gas naturally occurs in the nuclear regions dominated by the gravity of the NSC. A remarkable implication is that the inner radius of circumnuclear rings can be used to infer an upper limit to the SMBH sphere of influence.

We acknowledge the anonymous referee for the constructive comments that helped us improving the manuscript. We thank Sandro Bressan, Romain Teyssier, Roberto Capuzzo Dolcetta, Monica Colpi and Andi Burkert for interesting discussions. This work was supported by JSPS KAKENHI Grant Number 17F17764. AAT and MM acknowledge financial support from INAF through grant PRIN-2014-14 (Star formation and evolution in galactic nuclei). MM and AB acknowledge financial support from Fondation MERAC. The initial conditions were generated using the AMUSE framework (Portegies Zwart et al. 2009, 2013; Pelupessy et al. 2013). All plots were made with the Veusz plotting package. The simulations were run on the Ulysses cluster at SISSA.

APPENDIX

IMPACT OF CLOUD SIZE AND ORBIT

We have run two sets of simulations to explore the impact of initial size and orbit of the cloud on the final outcome. One set features the disruption of a compact cloud of radius $R_{\text{cloud}} = 5 \text{ pc}$ and the same mass as the other clouds simulated in this paper, while for the second we simulate a cloud on a wider orbit by setting the initial velocity to $v_i = 0.8v_{\text{esc}}$. For both sets, we choose $M_{\text{tot}} = 5 \times 10^6 M_{\odot}$ and $f_{\text{SMBH}} = M_{\text{SMBH}}/M_{\text{tot}} = 0.5, 0.2, 0.1$, for a total of 8 simulations. The initial conditions are listed in Table 3. We expect that little gas will be captured by the SMBH in the simulations with $f_{\text{SMBH}} < 0.5$ because of the lack of low-angular momentum gas particles.

Figure 6 shows the projected density map of gas for all 8 supplementary simulations. For $v_i = 0.8v_{\text{esc}}$, the outer ring forms at much larger radius than in the simulations with $v_i = 0.2v_{\text{esc}}$ (bottom row of Figure 1). It is also apparent that the lower the SMBH mass, the farther out the ring settles down. This indicates that even if the tidal disruption occurs outside R_{SOI} , the final radius of the ring can still be affected by the presence of the SMBH. In none of the simulations with $f_{\text{SMBH}} < 0.5$ an inner disk forms inside R_{SOI} .

In the simulations with $R_{\text{cloud}} = 5 \text{ pc}$, the cloud takes longer to be disrupted and settle around the SMBH due to the higher density and compactness. As in the $v_i = 0.8v_{\text{esc}}$ cases, no inner disk forms in the simulations with $f_{\text{SMBH}} < 0.5$. The lack of gas within R_{SOI} is to be attributed to the lack of low-angular momentum particles compared to the $R_{\text{cloud}} = 15 \text{ pc}$ simulations.

The disk in the $f_{\text{SMBH}} = 0.5$ simulation (bottom-left panel of Figure 6) is comparable in size to the disk in the $R_{\text{cloud}} = 15 \text{ pc}$ case. On the other hand, the radius of the rings in the simulations with $f_{\text{SMBH}} < 0.5$ is larger than in the $R_{\text{cloud}} = 15 \text{ pc}$ case. This indicates that for $R_{\text{cloud}} = 5 \text{ pc}$ and $f_{\text{SMBH}} < 0.5$, the angular momentum transport is less efficient. This might be due to the narrow spread in impact parameter of individual gas particles, which leads to a narrow distribution of the initial angular velocities. Since here the angular momentum transport arises from shear flow, the viscous torque is proportional to the gradient of the angular velocity, which is shallower for a more compact cloud.

Nonetheless, these simulations display the same qualitative behaviour of those presented in Section 3, i.e. a ring forms outside the sphere of influence of the SMBH, while a disk tends to form inside it.

REFERENCES

- Alig, C., Burkert, A., Johansson, P. H., & Schartmann, M. 2011, MNRAS, 412, 469
 Bahcall, J. N., & Wolf, R. A. 1976, ApJ, 209, 214
 —. 1977, ApJ, 216, 883
 Barth, A. J., Boizelle, B. D., Darling, J., et al. 2016a, ApJ, 822, L28
 Barth, A. J., Darling, J., Baker, A. J., et al. 2016b, ApJ, 823, 51
 Bartko, H., Martins, F., Fritz, T. K., et al. 2009, ApJ, 697, 1741

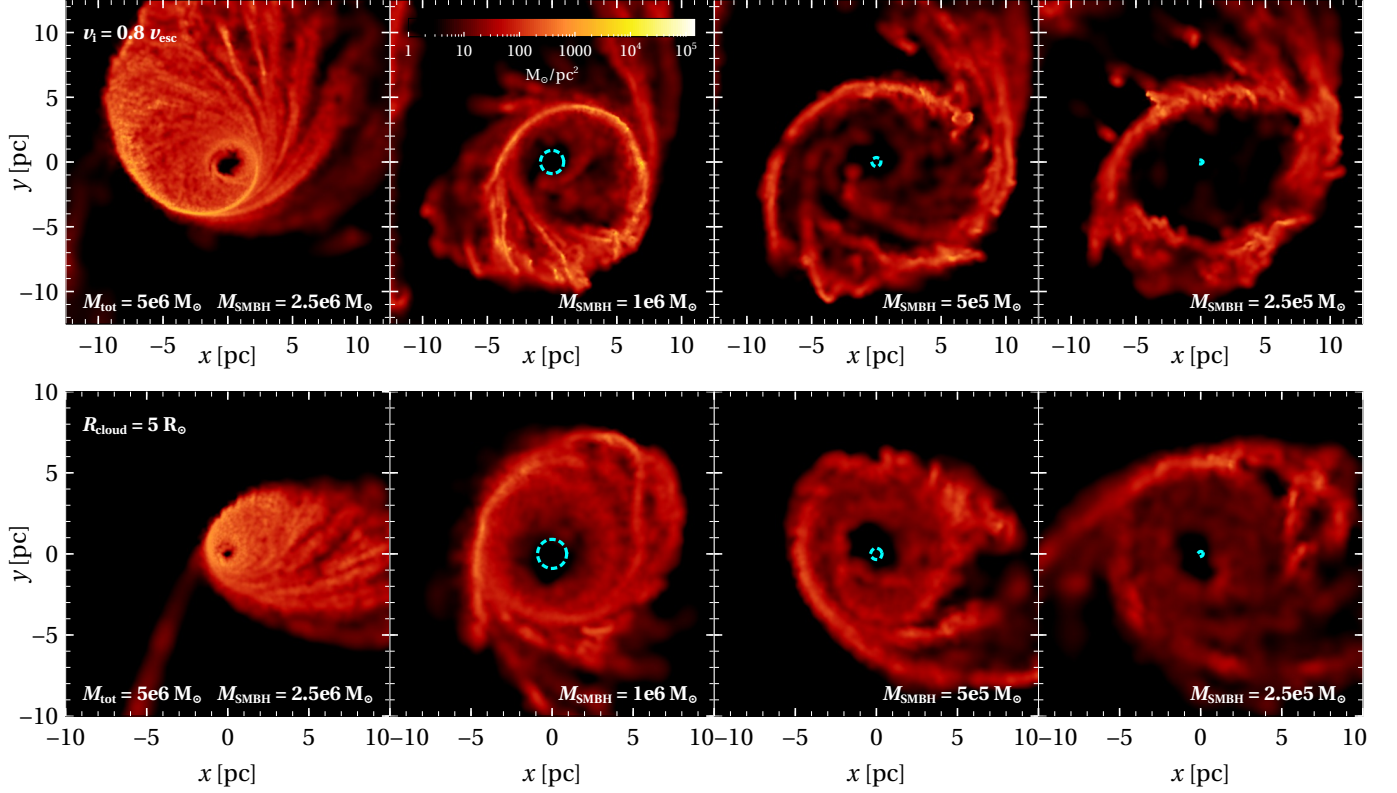


FIG. 6.— Color-coded, projected density map of gas in the x - y plane for the 8 supplementary simulations (see Table 3). Top and bottom rows show simulations with $v_i = 0.8v_{\text{esc}}$ and $R_{\text{cloud}} = 5 \text{ pc}$, respectively. From left to right, each column has $f_{\text{SMBH}} = M_{\text{SMBH}}/M_{\text{tot}} = 0.5, 0.2, 0.1$ and 0.05 . All simulations consist of $M_{\text{tot}} = M_{\text{cusp}} + M_{\text{SMBH}} = 5 \times 10^6 M_{\odot}$. The dashed cyan circle indicates the SMBH radius of influence R_{SOI} . Top (bottom) row corresponds to a time of 3 (4.5 Myr) from the start of the simulations. R_{SOI} is not shown in the left-hand panels because it is larger than the box.

TABLE 3
PROPERTIES OF THE SUPPLEMENTARY SIMULATIONS.

Run	$M_{\text{tot}} [M_{\odot}]$	$M_{\text{SMBH}} [M_{\odot}]$	f_{SMBH}	$R_{\text{SOI}} [\text{pc}]$	v_i/v_{esc}	$R_{\text{cloud}} [\text{pc}]$
mt5e6_bh2.5e6	5×10^6	2.5×10^6	0.5	>10	0.8	15
mt5e6_bh1e6	5×10^6	1×10^6	0.2	0.90	0.8	15
mt5e6_bh5e5	5×10^6	5×10^5	0.1	0.35	0.8	15
mt5e6_bh2.5e5	5×10^6	2.5×10^5	0.05	0.15	0.8	15
mt5e6_bh2.5e6	5×10^6	2.5×10^6	0.5	>10	0.2	5
mt5e6_bh1e6	5×10^6	1×10^6	0.2	0.90	0.2	5
mt5e6_bh5e5	5×10^6	5×10^5	0.1	0.35	0.2	5
mt5e6_bh2.5e5	5×10^6	2.5×10^5	0.05	0.15	0.2	5

Column 1: run name; column 2: mass enclosed in a 10 pc radius M_{tot} in M_{\odot} , composed of the NSC and the SMBH; column 3: mass of the SMBH M_{SMBH} in M_{\odot} ; column 4: mass of the SMBH with respect to total mass enclosed f_{SMBH} ; column 5: radius of sphere of influence R_{SOI} of the SMBH in pc; m_{res} is the mass resolution of the simulation in M_{\odot} .

Bate, M. R., Bonnell, I. A., & Price, N. M. 1995, MNRAS, 277, 362
 Bender, R., Kormendy, J., Bower, G., et al. 2005, ApJ, 631, 280
 Böker, T., Laine, S., van der Marel, R. P., et al. 2002, AJ, 123, 1389
 Böker, T., Sarzi, M., McLaughlin, D. E., et al. 2004, AJ, 127, 105
 Boley, A. C. 2009, ApJ, 695, L53
 Boley, A. C., Hayfield, T., Mayer, L., & Durisen, R. H. 2010, Icarus, 207, 509
 Bonnell, I. A., & Rice, W. K. M. 2008, Science, 321, 1060
 Brown, C. K., & Magorrian, J. 2013, MNRAS, 431, 80
 Carson, D. J., Barth, A. J., Seth, A. C., et al. 2015, AJ, 149, 170
 Chatzopoulos, S., Fritz, T. K., Gerhard, O., et al. 2015, MNRAS, 447, 948
 Christopher, M. H., Scoville, N. Z., Stolovy, S. R., & Yun, M. S. 2005, ApJ, 622, 346
 Collin, S., & Zahn, J.-P. 1999, A&A, 344, 433
 —. 2008, A&A, 477, 419

Côté, P., Piatek, S., Ferrarese, L., et al. 2006, ApJS, 165, 57
 Cuadra, J., Armitage, P. J., & Alexander, R. D. 2008, MNRAS, 388, L64
 Cullen, L., & Dehnen, W. 2010, MNRAS, 408, 669
 Dale, J. E., Ercolano, B., & Bonnell, I. A. 2015, MNRAS, 451, 987
 D’Alessio, P., Calvet, N., & Hartmann, L. 2001, ApJ, 553, 321
 Davis, T. A. 2014, MNRAS, 443, 911
 Davis, T. A., Bureau, M., Cappellari, M., Sarzi, M., & Blitz, L. 2013, Nature, 494, 328
 Davis, T. A., Bureau, M., Onishi, K., et al. 2017, MNRAS, 468, 4675
 —. 2018, MNRAS, 473, 3818
 den Brok, M., Peletier, R. F., Seth, A., et al. 2014, MNRAS, 445, 2385
 Do, T., Lu, J. R., Ghez, A. M., et al. 2013, ApJ, 764, 154
 Do, T., Wright, S. A., Barth, A. J., et al. 2014, AJ, 147, 93
 Dubinski, J., Narayan, R., & Phillips, T. G. 1995, ApJ, 448, 226

- Eisenhauer, F., Genzel, R., Alexander, T., et al. 2005, *ApJ*, 628, 246
- Espada, D., Matsushita, S., Miura, R. E., et al. 2017, *ArXiv e-prints*, arXiv:1706.05762
- Federrath, C., Banerjee, R., Clark, P. C., & Klessen, R. S. 2010, *ApJ*, 713, 269
- Feldmeier, A., Neumayer, N., Seth, A., et al. 2014, *A&A*, 570, A2
- Feldmeier-Krause, A., Kerzendorf, W., Neumayer, N., et al. 2017, *MNRAS*, 464, 194
- Feldmeier-Krause, A., Neumayer, N., Schödel, R., et al. 2015, *A&A*, 584, A2
- Fritz, T. K., Chatzopoulos, S., Gerhard, O., et al. 2016, *ApJ*, 821, 44
- Gallego-Cano, E., Schödel, R., Dong, H., et al. 2017, *ArXiv e-prints*, arXiv:1701.03816
- Gammie, C. F. 2001, *ApJ*, 553, 174
- Genzel, R., Schödel, R., Ott, T., et al. 2003a, *ApJ*, 594, 812
- . 2003b, *ApJ*, 594, 812
- Georgiev, I. Y., & Böker, T. 2014, *MNRAS*, 441, 3570
- Georgiev, I. Y., Böker, T., Leigh, N., Lützgendorf, N., & Neumayer, N. 2016, *MNRAS*, 457, 2122
- Ghez, A. M., Duchêne, G., Matthews, K., et al. 2003, *ApJ*, 586, L127
- Gillessen, S., Eisenhauer, F., Fritz, T. K., et al. 2009a, *ApJ*, 707, L114
- Gillessen, S., Eisenhauer, F., Trippe, S., et al. 2009b, *ApJ*, 692, 1075
- Gillessen, S., Plewa, P. M., Eisenhauer, F., et al. 2017, *ApJ*, 837, 30
- Goicoechea, J. R., Pety, J., Chapillon, E., et al. 2018, *ArXiv e-prints*, arXiv:1806.01748
- Goicoechea, J. R., Etxaluze, M., Cernicharo, J., et al. 2013, *ApJ*, 769, L13
- Goodman, J. 2003, *MNRAS*, 339, 937
- Graham, A. W., & Spitler, L. R. 2009, *MNRAS*, 397, 2148
- Gullieuszik, M., Greggio, L., Falomo, R., Schreiber, L., & Uslenghi, M. 2014, *A&A*, 568, A89
- Harada, N., Riquelme, D., Viti, S., et al. 2015, *Astronomy & Astrophysics*, 584, A102
- Hobbs, A., & Nayakshin, S. 2009, *MNRAS*, 394, 191
- King, I. 1962, *AJ*, 67, 471
- Kolykhalov, P. I., & Syunyaev, R. A. 1980, *Soviet Astronomy Letters*, 6, 357
- Kormendy, J., & Ho, L. C. 2013, *ARA&A*, 51, 511
- Kornei, K. A., & McCrady, N. 2009, *ApJ*, 697, 1180
- Larson, R. B. 1981, *MNRAS*, 194, 809
- Lauer, T. R., Bender, R., Kormendy, J., Rosenfield, P., & Green, R. F. 2012, *ApJ*, 745, 121
- Levin, Y., & Beloborodov, A. M. 2003, *ApJ*, 590, L33
- Liu, H. B., Ho, P. T. P., Wright, M. C. H., et al. 2013, *The Astrophysical Journal*, 770, 44
- Liu, H. B., Hsieh, P.-Y., Ho, P. T. P., et al. 2012, *The Astrophysical Journal*, 756, 195
- Lockhart, K. E., Lu, J. R., Peiris, H. V., et al. 2017, *ArXiv e-prints*, arXiv:1710.01394
- Lucas, W. E., Bonnell, I. A., Davies, M. B., & Rice, W. K. M. 2013, *MNRAS*, 433, 353
- Mapelli, M. 2017, *MNRAS*, 467, 3255
- Mapelli, M., Hayfield, T., Mayer, L., & Wadsley, J. 2008, *ArXiv e-prints*, arXiv:0805.0185
- . 2012, *ApJ*, 749, 168
- Mapelli, M., & Trani, A. A. 2016, *A&A*, 585, A161
- Menezes, R. B., & Steiner, J. E. 2015, *ApJ*, 808, 27
- Menezes, R. B., Steiner, J. E., & Ricci, T. V. 2013, *ApJ*, 762, L29
- Mills, E. A. C., Güsten, R., Requena-Torres, M. A., & Morris, M. R. 2013, *The Astrophysical Journal*, 779, 47
- Mills, E. A. C., Togi, A., & Kaufman, M. 2017, *ArXiv e-prints*, arXiv:1701.04826
- Milosavljević, M. 2004, *ApJ*, 605, L13
- Nayakshin, S., & Cuadra, J. 2005, *A&A*, 437, 437
- Nayakshin, S., Cuadra, J., & Springel, V. 2007, *MNRAS*, 379, 21
- Neumayer, N., Cappellari, M., Reunanen, J., et al. 2007, *ApJ*, 671, 1329
- Nguyen, D. D., Seth, A. C., Neumayer, N., et al. 2017, *ArXiv e-prints*, arXiv:1711.04314
- Oka, T., Nagai, M., Kamegai, K., & Tanaka, K. 2011, *The Astrophysical Journal*, 732, 120
- Onishi, K., Iguchi, S., Davis, T. A., et al. 2017, *MNRAS*, 468, 4663
- Onishi, K., Iguchi, S., Sheth, K., & Kohno, K. 2015, *ApJ*, 806, 39
- Paumard, T., Genzel, R., Martins, F., et al. 2006, *ApJ*, 643, 1011
- Pelupessy, F. I., & Portegies Zwart, S. 2012, *MNRAS*, 420, 1503
- Pelupessy, F. I., van Elteren, A., de Vries, N., et al. 2013, *A&A*, 557, A84
- Poliachenko, V. L., & Shukhman, I. G. 1977, *Soviet Astronomy Letters*, 3, 134
- Portegies Zwart, S., McMillan, S. L. W., van Elteren, E., Pelupessy, I., & de Vries, N. 2013, *Computer Physics Communications*, 184, 456
- Portegies Zwart, S., McMillan, S., Harfst, S., et al. 2009, *NewA*, 14, 369
- Read, J. I., Hayfield, T., & Agertz, O. 2010, *MNRAS*, 405, 1513
- Sanders, R. H. 1998, *MNRAS*, 294, 35
- Sandqvist, A., Hjalmarsen, Å., Frisk, U., et al. 2017, *A&A*, 599, A135
- Schödel, R., Feldmeier, A., Kunneriath, D., et al. 2014, *A&A*, 566, A47
- Schödel, R., Gallego-Cano, E., Dong, H., et al. 2017, *ArXiv e-prints*, arXiv:1701.03817
- Schödel, R., Merritt, D., & Eckart, A. 2009, *A&A*, 502, 91
- Schödel, R., Ott, T., Genzel, R., et al. 2003, *ApJ*, 596, 1015
- . 2002, *Nature*, 419, 694
- Schödel, R., Eckart, A., Alexander, T., et al. 2007, *A&A*, 469, 125
- Serabyn, E., Guesten, R., Walmsley, J. E., Wink, J. E., & Zylka, R. 1986, *A&A*, 169, 85
- Seth, A., Agüeros, M., Lee, D., & Basu-Zych, A. 2008, *ApJ*, 678, 116
- Seth, A. C. 2010, *ApJ*, 725, 670
- Shlosman, I., & Begelman, M. C. 1987, *Nature*, 329, 810
- Smith, I. L., & Wardle, M. 2014, *MNRAS*, 437, 3159
- Takekawa, S., Oka, T., & Tanaka, K. 2017, *ApJ*, 834, 121
- Trani, A. A., Mapelli, M., Bressan, A., et al. 2016, *ApJ*, 818, 29
- Tremaine, S. 1995, *AJ*, 110, 628
- Tristram, K. R. W., Raban, D., Meisenheimer, K., et al. 2009, *A&A*, 502, 67
- Wadsley, J. W., Keller, B. W., & Quinn, T. R. 2017, *ArXiv e-prints*, arXiv:1707.03824
- Wadsley, J. W., Stadel, J., & Quinn, T. 2004, *NewA*, 9, 137
- Wardle, M., & Yusef-Zadeh, F. 2008, *ApJ*, 683, L37
- Wright, M. C. H., Coil, A. L., McGary, R. S., Ho, P. T. P., & Harris, A. I. 2001, *ApJ*, 551, 254
- Yelda, S., Ghez, A. M., Lu, J. R., et al. 2014, *ApJ*, 783, 131
- Yoon, I. 2017, *MNRAS*, 466, 1987
- Yusef-Zadeh, F., Bushouse, H., & Wardle, M. 2012, *ApJ*, 744, 24
- Yusef-Zadeh, F., Cotton, B., Wardle, M., et al. 2017a, *MNRAS*, 467, 922
- Yusef-Zadeh, F., Roberts, D. A., Wardle, M., et al. 2015, *ApJ*, 801, L26
- Yusef-Zadeh, F., Wardle, M., Kunneriath, D., et al. 2017b, *ApJ*, 850, L30
- Yusef-Zadeh, F., Royster, M., Wardle, M., et al. 2013, *ApJ*, 767, L32